Reaction Rates and Dissolution Mechanisms of Quartz as a Function of pH†

Shikha Nangia and Barbara J. Garrison*

104 Chemistry Building, Department of Chemistry, The Pennsylvania State University, University Park, Pennsylvania 16802

Received: August 3, 2007; In Final Form: November 13, 2007

In this computational study, we present the dissolution rates for quartz as a function of pH at 298 K. At any given pH, the dissolution of the quartz surface depends on the distribution of protonated, deprotonated, or neutral species. The dissolution mechanism for each of these three species was investigated by *ab initio* electronic structure calculations to obtain the reaction profile. Using the barrier height along with the partition functions for the transition state and the reactants in the rate-limiting steps, we calculated the TST rate constants for the reactions for the temperature range of 200−500 K. At 298 K the rate constant (s^{-1}) for the dissolution of neutral species was found to be several orders of magnitude smaller than the rate-limiting steps for the protonated and deprotonated species. The values of the rate constants were used in the rate law expression to calculate the overall dissolution rate (mol m^{-2} s^{-1}) at a given pH. The calculated rates were compared to previously reported experimental and theoretical rates and were found to be in good agreement over 2−12 pH range.

I. Introduction

One of the most common geochemical processes that occurs on earth's surface is the dissolution of rocks and minerals by water.[1] The global water cycle, environmental pollution, and acid rain are some of the factors that contribute toward accelerating the mineral-water dissolution process. Among all the minerals, silicates comprise the largest group of minerals, and as a result, they attract considerable interest from geochemists. In addition, silicates have multiple technological applications in the chemical industry including semiconductors, microelectronics, zeolite synthesis, glass, adhesives, and paints.[2−4] All these applications have led to numerous experimental[5−13] and computational[14−30] studies focused on understanding the interactions at the silica-water interface.

The bulk of silica is composed of Si−O−Si linkages, but the surface terminations consist of hydrophilic hydroxyl groups. The silica surfaces interact with water in two competing processes of physical adsorption and chemical dissolution. In the physical process, the hydroxyl groups adsorb water molecules by hydrogen bonding, sometimes forming stable tessellated patterns;[25,30] however, in the chemical process water interacts with the surface to cleave the Si−O−Si linkages, resulting in hydrolyzed products. In both processes the role of surface hydroxyl groups is significant, and there have been experimental studies[31,32] to detect these groups. The nature of the surface hydroxyl groups varies depending upon the porosity, particle size, crystal faces, and the pH.[30,33−42] The change in pH alters the protonation state of the surface groups, significantly affecting the dissolution mechanism and the reaction rate.

The dependence of the dissolution rate on pH can be explained by the change in the characteristics and distribution of the surface reaction sites. Under ambient conditions, the hydroxyl groups on the quartz surface interact with water to form neutral and ionized forms that can be written as

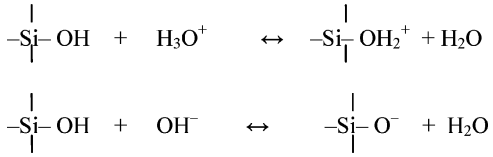

where ≡$SiOH_2^+$, ≡SiOH, and ≡SiO^- represent the protonated, neutral, and deprotonated surface sites. The presence of more than one type of surface species implies that there can be multiple reaction mechanisms occurring on the quartz surface during dissolution. The surface sites differ in their polarity and reactivity toward hydrolysis. The overall reactivity of the quartz surface depends on the relative distribution of the three species which changes with the pH affecting the overall rate of the dissolution process. Studies by Knauss and Wolery[43] have shown that the reaction rate for quartz increases by 4 orders of magnitude at pH range above 7, and on the low end of the pH scale, the rates were less sensitive to the change in pH. These experimental observations show that the silica dissolution mechanisms change significantly over the entire pH scale.

In computational studies, the focus has been to determine reaction pathways in acid[17,23,24,29,44] and basic media.[16,18] Xiao and Lasaga[17,18] studied the catalytic effects of H_3O^+ and OH^- on silicate dissolution and concluded that the barrier to the reaction in acidic and basic conditions is much smaller than in the neutral medium. Xiao and Lasaga also showed that in protonation of Si−O−Si group occurs at the bridging oxygen atom compared to the terminal hydroxyl,[16] and this has been accepted and used in more recent work by Criscenti and coworkers.[28] In the deprotonated case, the generally accepted mechanism is the direct attack of water on the surface followed by the catalysis of the neutral site by the OH^- ion.[16,18] Although these studies focus on the reaction profiles and the barrier heights, they do not address the overall dissolution process. The data presented in refs 17 and 18 show the hydrolysis of Si−O−Si bond either in neutral medium or in extremely acidic and basic conditions. However, as mentioned previously, a distribu-

† Part of the "William A. Lester, Jr., Festschrift".

10.1021/jp076243w CCC: $40.75
Published on Web 01/23/2008

tion of protonated, neutral, and deprotonated surface sites exist at each pH, and the contribution from all these three species is essential to understand the overall dissolution rate.

There have been Si−O−Si hydrolysis studies of β-cristobalite by single water molecule in the gas phase using the cluster approach.[23,24] The calculations estimated the energy barrier for dissolution of $Si(OH)_4$ for doubly-, triply-, quadruply bridged Si species to be 96, 138, 205 kJ/mol, respectively. The increase in the barrier with increase in Si connectivity is attributed to the increase resistance of lattice to relaxation of the activated complex of the reaction. The dissolution, however, occurs on the surface where surface relaxation is possible should be dominated by the dissociation from Si center with the lowest connectivity. It is also proposed that dissolution occurs at specific sites on the cleavage planes, corners, and edges where the connectivity of the Si sites is lower.[45]

The purpose of this study is to understand the differences in the mechanisms for protonated, neutral, and deprotonated surface species and compute the contribution from each of them to the overall dissolution rate. At any given pH, the overall rate calculation requires the values of the rate constant and the surface fractions as input quantities. The values of the rate constant depend on the barrier height of the rate-limiting step and are calculated for each of the surface species. The approach of the present work is to provide a comprehensive investigation of rate-limiting steps of the dissolution process and to calculate the reaction rates at each pH.

II. Theory

The *ab initio* approach allows us to identify the sequence of elementary reactions that comprise of the overall dissolution process. In a series of sequential reactions, the slowest step determines the rate of the reaction and is called the rate-limiting step. The rate-limiting step is a dynamical bottleneck for the reaction, and the value of the rate constant depends on the barrier height of the transition state for that step. The transition state of a reaction is the highest energy point on the minimum energy path that connects the reactants to the products, and the activation energy required to cross the transition state from the reactants is the barrier to the forward reaction. At the transition state structure, we can define a dividing surface normal to the reaction coordinate that separates the phase space into the reactant region and the product region. The knowledge of the activation barrier for the reaction and the partition functions of the reactant and transition state at a given temperature are sufficient to calculate the thermal rate constants of a reaction using transition state theory (TST).

There are several ways to derive the fundamental equations of transition state theory, but in the present work we will present the mathematical expression of the TST rate constant and a brief discussion of the basic assumptions needed to derive the TST expression. The TST expression for the rate constant is

$$k^{\ddagger}(T) = \frac{k_B T}{h} \frac{Q^{\ddagger}(T)}{Q(T)} e^{-V^{\ddagger}/k_B T} \quad (1)$$

where $V^{\ddagger}$ is the barrier height of the reaction, $Q^{\ddagger}$ is the partition function of the transition state, Q is the partition function of the reactants, k_B is Boltzmann's constants, h is Planck's constant, and T is the temperature. The reactant and the transition state partition functions are computed by taking a product of vibrational and rotational partition functions. The rigid-rotator approximation was applied for rotational motion and all bound vibrational degrees of freedom were assumed to be harmonic. Though in its earliest formulation, the TST rate constant equation had the classical partition functions for reactants and transition state, later the quantum effects were included by substituting the quantum partition functions in the rate expression. Another important assumption is that the dividing surface defined at the transition state is a dynamical bottleneck such that every trajectory passing through the dividing surface cannot re-cross; i.e., all trajectories originating in the reactant region proceed to products and vice-versa without ever returning to the dividing surface. This assumption is crucial and gives an upper bound to the calculation of the rate constant. There have been several modifications to variationally choose the transition state and improve the conventional transition state theory,[46] but in this primary investigation of calculating rate constants for silica clusters, we will restrict our discussion to the TST calculations. The improved effects of variational transition state theory will be included in the subsequent studies.

The rate of a reaction can be expressed as the rate of disappearance of the reactants or as rate of appearance of products. In the case of dissolution of minerals, generally the rate of increase of product concentration is measured experimentally using batch, flow-through, and fluid bed reactors.[47,48] experiments. The rate of dissolution is expressed in the units of dissolution of the phase per surface area per unit time (mol m^{-2} s^{-1}).

Theoretical investigation of the dissolution rate relies on the calculation of the reaction rate constant. The relationship between the dissolution rate and rate constant is well-known and is mathematically written as[49]

$$r = k\rho \quad (2)$$

where k is the rate constant (s^{-1}) of the reaction and ρ is the molar surface density (mol m^{-2}) of the mineral surface. It is important to note that dissolution occurs at specific reaction sites on the mineral surface and depending on pH of the solution, the nature of the reactive site and thus the effective surface density can change significantly. In the case of silicates, the mole fractions of $\equiv SiOH_2^+$, $\equiv SiOH$, and $\equiv SiO^-$ surface sites can be calculated on the basis of the temperature and the ionization reactions of silica.[50] The overall rate expression is written as the sum of the contributions from each of the surface species as

$$r = k_{\equiv SiOH_2^+}\theta_{\equiv SiOH_2^+}\rho + k_{\equiv SiOH}\theta_{\equiv SiOH}\rho + k_{\equiv SiO^-}\theta_{\equiv SiO^-}\rho \quad (3)$$

where $k_{\equiv SiOH_2^+}$ is the dissolution rate constant of the protonated species, $k_{\equiv SiOH}$ is the dissolution rate constant of the neutral species, $k_{\equiv SiO^-}$ is the dissolution rate constant of the deprotonated species, $\theta_{\equiv SiOH_2^+}$ is the fraction of the protonated surface sites, $\theta_{\equiv SiOH}$ is the fraction of the neutral surface sites, $\theta_{\equiv SiO^-}$ is the fraction of the deprotonated surface sites, and ρ is the molar surface density of reactive sites.

For quartz the total number of reactive surface sites (or surface hydroxyl groups) are 5−7 nm^{-2}. It is important to note that $\theta_{\equiv SiOH_2^+}$, $\theta_{\equiv SiOH}$, and $\theta_{\equiv SiO^-}$ are fractions of the total reactive sites on the quartz surface, and their sum is equal to one. The rate expression in eq 3 does not distinguish the surface sites on the connectedness (number of bridging oxygen bonds) of the tetrahedrally coordinated silicon atoms on the surface. The rate calculations in this work will focus only on the protonated, neutral, and deprotonated species predominant on the quartz surface and relate values of the rate of reaction to pH.

TABLE 1: Selected Bond Lengths (Å) and Angle (deg) Parameters of Clusters Calculated Using the 6-31+G(d,p) Basis Set

cluster	no. of atoms	Si−O	Si−O_{br}	Si−O_{br}−Si	Si−O−H
protonated	16	1.636	1.734	130.7	120.3
neutral	15	1.63	1.619	148.9	118.2
deprotonated	14	1.569, 1.671	1.674	126.5	110.2, 112.3

III. Computational Method

We begin the study of the dissolution process with the *ab initio* investigation of the protonated, neutral, and deprotonated reactions for a silica cluster. More specifically, the protonated, neutral, and deprotonated reactions considered in this work are

$$(OH)_3Si{-}O{-}Si(OH)_3\,H^+ + H_2O \rightarrow (OH)_3Si{-}OH + Si(OH)_3{-}OH_2^+ \quad (R1)$$

$$(OH)_3Si{-}O{-}Si(OH)_3 + H_2O \rightarrow (OH)_3Si{-}OH + (OH)_3Si{-}OH \quad (R2)$$

$$(OH)_3Si{-}O{-}Si(OH)_2O^- + H_2O \rightarrow (OH)_3Si{-}OH + (OH)_3Si{-}O^- \quad (R3)$$

respectively. In Table 1, selected bond distances and bond angle parameters are provided for each of the three reactant clusters in R1−R3 reactions. The clusters are all terminated with the hydroxyl groups as

It is important to note that in the R1 reaction, the protonation of the silicate preferentially occurs on the bridged oxygen atom. This was first shown by Xiao and Lasaga,[17] and later used in acid hydrolysis studies[29] that the adsorption of H^+ on bridging oxygen is thermodynamically more favorable. Using electronic structure theory calculations, we identify the elementary steps of the reactions, characterize the transition states and intermediates, calculate the reaction barriers, and determine the rate-limiting steps.

It is important for any *ab initio* calculation that the quantities such as geometries, frequencies, and barrier heights are determined accurately. There are two classes of *ab initio* methods, namely, the wave function theory (WFT) and the density functional theory (DFT). The DFT methods account for the electron correlation energy through the exchange-correlation functional and there are several functionals available in the literature. The most commonly used functional is the B3LYP[51−54] based on the names of Becke−Lee−Yang−Parr. The B3LYP functional provides a good balance of computational cost and accuracy and has been shown to require much smaller basis sets than the WFT methods.[55] The other aspect of an *ab initio* calculation is the choice of basis set. One of the earlier basis sets that has been widely used for its affordability is the 6-31+G(d,p) basis set. It is an all-electron type basis set developed by Pople and co-workers.[56] Another useful all-electron type basis set is the MG3 semi-diffuse (MG3S),[57] derived from the earlier MG3 basis set.[58,59] For oxygen the MG3 basis set is identical to 6-311++G(2df,2p), for hydrogen it is similar to 6-311++G(3d,2f) with the diffuse functions removed, and for silicon it is 6-311++(3d,2f). A detailed study of the computational requirements for study of siliceous materials was carried out by Zhang et al.[55] where the MG3S basis set with several DFT functionals was shown to be useful for computing several geometric and energetic quantities that were in good agreement with the experimental data.

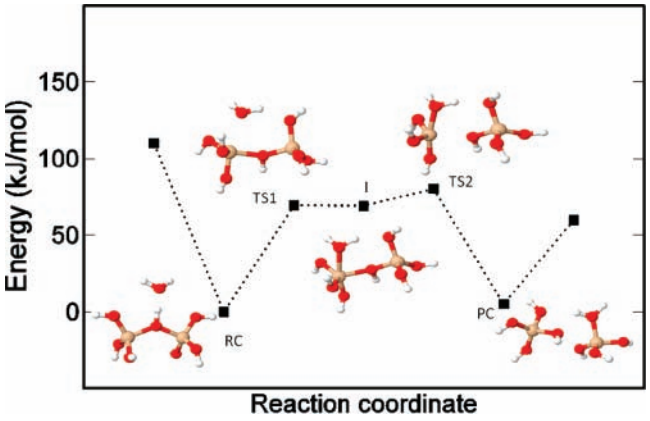

Figure 1. Energy profile (kJ/mol) of the Si−O−Si hydrolysis reaction along the reaction coordinates for the protonated species. The geometries of the reactant complex (RC), first transition state (TS1), intermediate (I), second transition state (TS2), and the product complex (PC) are shown along the path. The Si, O, and H atoms are shown in light brown, red, and white colors, respectively. The zero of energy is defined at the RC geometry.

In the present calculations, geometry optimization and frequency calculations were performed using the density functional theory method in the GAUSSIAN 03 package.[60] The B3LYP hybrid exchange-correlation functional was used with the 6-31+G(d,p) and MG3S basis sets. The implicit solvation calculations were performed using the integral equation formalism for the polarizable continuum model[61] (IEFPCM) for self-consistent reaction field available in GAUSSIAN 03. The aim is to use affordable computation methods, such as density functional theory, that provide accurate results with the smallest possible basis set. Both basis sets are tested in the present calculations to compare their accuracies and to determine the basis set of choice for larger silica clusters in future calculations.

The rate calculations were performed using the GAUSSRATE[62] program that provides an interface between the POLYRATE[63] and GAUSSIAN 03 programs. The GAUSSRATE program facilitates the flow of data of the optimized reactants, products, and transition states from GAUSSIAN 03 to POLYRATE for the dynamical rate calculations. The POLYRATE program uses conventional and variational transition state theory and semiclassical tunneling calculations to compute chemical reaction rates of gas-phase reactions. The method to calculate rate constants in POLYRATE can be based on a potential energy function or interpolated from electronic structure data along a minimum energy path. In the present calculations the optimized structures of the reactants, products, and transition states were provided from *ab initio* calculations. The rate constants were calculated for reactions R1−R3 and will be presented in the following section.

IV. Results and Discussion

IV.A. Reaction Mechanisms. The dissolution process at a protonated site on the silica surface is described by considering the interaction between the protonated silica cluster and water in reaction R1. The reaction proceeds through two transition states and a stable intermediate as shown in Figure 1. The initial step of the reaction is the formation of a stable hydrogen-bonded reaction complex (RC) where the proton is bonded to the electron-rich bridged oxygen of the Si−O_{br}−Si bond, forming a highly stabilized complex with C_{2v} symmetry. For hydrolysis, the C_{2v} symmetry breaks followed by a conformation change to allow water to coordinate with the Si atom and form the first transition state (TS1). This conformational change requires 69

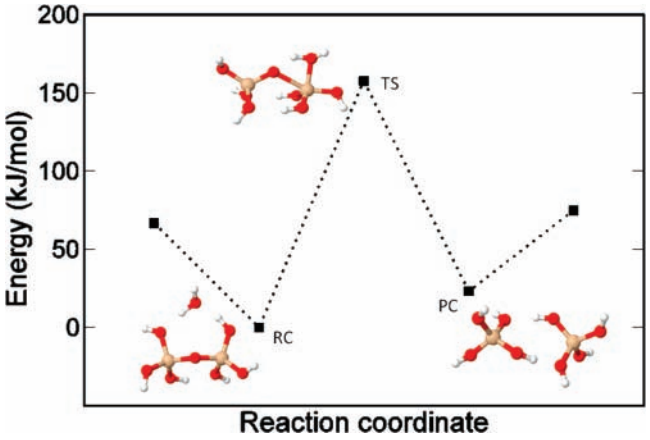

Figure 2. Energy profile (kJ/mol) of the Si−O−Si hydrolysis reaction along the reaction coordinates for the neutral species. The geometries of the reactant complex (RC), transition state (TS), and product complex (PC) are shown along the path. The Si, O, and H atoms are shown in light brown, red, and white colors, respectively. The zero of energy is defined at the RC geometry.

TABLE 2: Barrier Heights (kJ/mol) for the Hydrolysis of the Si−O−Si Bond in Protonated, Neutral, and Deprotonated Reaction Sites in the Gas Phase and Implicit Water Solvent Calculated Using the B3LYP Method with 6-31+G(d,p) and MG3S (Shown in Parentheses) Basis Sets

	gas phase		water		refs 17 and 18[a]
	TS1	TS2	TS1	TS2	
protonated	69 (75)	12 (18)	65 (72)	11 (9)	100
neutral	159 (174)		147 (162)		121
deprotonated	110 (122)	22 (31)	90 (101)	26 (32)	79

[a] Obtained using MP2 theory with the 6-31*G basis set.

kJ/mol of energy and is the barrier height of the reaction. The imaginary mode for the first transition state is the water attaching to the Si center. The TS1 leads to the formation of penta-coordinated Si intermediate with water coordinated at the equatorial positions of the trigonal-bipyramidal (tbp) geometry. In the next step, the intermediate leads to the formation of TS2 with a 12 kJ/mol barrier height. The imaginary mode in the TS2 geometry corresponds to breaking of the Si−O_{br} bond. The dissociated products are hydrogen-bonded, forming a stable product complex (PC). The barrier height for both the transition states are listed in Table 2. From the data it is clear that TS1 is the rate-limiting step as the barrier across TS1 is five times higher than that for TS2.

In contrast to the reaction in the protonated species, the reaction profile for the hydrolysis of the Si−O_{br}−Si bond in the neutral species (reaction R2) has only one transition state as shown in Figure 2. In the initial step, the reactants approach each other and their interaction is stabilized by hydrogen-bonds resulting in the formation of a RC. The water molecule is held symmetrically by the hydroxyl groups of the silicate cluster by two hydrogen bonds with bond lengths of 1.91 and 1.89 Å. The Si−O_{br} bond length between the silicon atom and the bridged O_{br} in the RC geometry is 1.69 Å. In the next step, the stabilized complex leads to the high-energy TS structure with the water molecule covalently bonded to form a penta-coordinated Si tbp center. The transition state structure is characterized as a late transition state where the water is already bonded to the Si atom. The Si−O_{br} bond length is elongated to 1.81 Å, and the Si−O_{br}−Si bond angle increases to 156° compared to 143° in the RC geometry. The elongated bond distances and larger angle allows the hydrogen atom of the covalently bonded water molecule to transfer to the O_{br} atom of the Si−O_{br}−Si group.

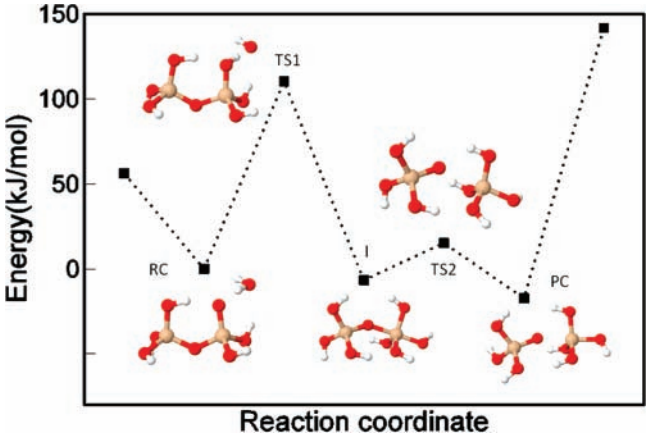

Figure 3. Energy profile (kJ/mol) of the Si−O−Si hydrolysis reaction along the reaction coordinates for deprotonated species. The notation is the same as in Figure 1.

TABLE 3: Reaction Rate Constants (s^{-1}) for the a Protonated, Neutral, and Deprotonated Surface Site on Quartz Calculated Using the 6-31+G(d,p) Basis Set

	protonated		neutral	deprotonated	
T (K)	TS1	TS2	TS	TS1	TS2
200	1.0E−07	1.2E+07	3.9E−28	2.2E−20	2.4E+05
298	6.6E−01	8.6E+08	6.5E−15	8.9E−05	1.0E+06
400	1.6E+03	2.3E+09	2.5E−08	5.4E−01	7.0E+07
500	7.7E+05	4.0E+10	2.3E−04	6.8E+02	2.2E+08

The barrier height of the reaction is 159 kJ/mol and is listed in Table 2. The unbound vibrational mode corresponds to two simultaneous bond-breaking processes (i.e., the O−H bond from water and the O_{br}−Si bond) and one bond making process (i.e., the O_{br}−H bond). The bond-breaking results in the formation of hydrogen-bonded product complex.

The reaction profile in the deprotonated species is very similar to that in the protonated species with two transition states and one intermediate, as shown in Figure 3. The initial step is the attack of the negatively charged silicate on water resulting in the formation of a stable hydrogen-bonded RC. The next step is the breaking of hydrogen bonds in the RC, followed by the transition state for the formation of the penta-coordinated Si center with a 110 kJ/mol barrier. Once formed the pentacoordinated Si species is a stable reaction intermediate. The next step is the breaking of the axial Si−O_{br} bridge bond in the TS2 geometry. The barrier for this bond-breaking process is 20 kJ/mol, smaller than for the TS1 step. The hydrolyzed products are stabilized by hydrogen bonds in the PC geometry.

To summarize, both the protonated and deprotonated reaction profiles have two transition states indicating a two-step process. In contrast, the neutral reaction is one-step process with concerted bond-breaking and bond-forming processes in the transition state. It is therefore not surprising that the barrier height for the neutral reaction is 90 and 49 kJ/mol higher than in the rate-limiting steps of the protonated and deprotonated species dissolution.

The data for geometries and barrier heights mentioned in the above discussion were obtained with the 6-31+G(d,p) basis set. All these geometries were reoptimized with the MG3S basis set, and the barrier heights for the three reactions increase by 4−13 kJ/mol. Table 2 lists the barrier heights for both basis sets in the present work along with the barrier height data reported by Xiao and Lasaga[17,18] using MP2 method with 6-31G* basis set. The implicit solvation calculations were carried out, and the barrier heights are shown in Table 2. The

TABLE 4: Comparison of Reported Quartz Dissolution Rates with the Rates Determined by *ab Initio* Rate Constant Calculations as a Function of pH

	surface fractions[a]			log rate (mol m^{-2} s^{-1})		
pH	protonated	neutral	deprotonated	expt	ref 64	this work
			Knauss and Wolery[43]			
2	0	0.99993	0	−12.9	−13.0	−10.8
3	0	0.99975	0	−12.8	−13.0	−12.0
4	0	0.98312	0.01688	−12.2	−12.3	−11.9
5	0	0.97560	0.02440	−11.5	−12.1	−11.7
6	0	0.86414	0.13586	−10.4	−10.9	−11.0
7	0	0.81598	0.18402	−10.4	−10.6	−10.9
8	0	0.79273	0.20727	−10.0	−10.5	−10.8
			Schwartentruber et al.[65]			
9.4	0	0.94916	0.05084	−11.9	−11.6	−11.4
9.7	0	0.92488	0.07512	−11.7	−11.3	−11.3
10.1	0	0.88720	0.11280	−11.4	−11.0	−11.1
10.4	0	0.85635	0.14365	−11.3	−10.8	−11.0
10.7	0	0.82425	0.17575	−11.1	−10.7	−10.9
11.0	0	0.78620	0.21380	−10.8	−10.5	−10.8
11.3	0	0.75680	0.24320	−10.8	−10.4	−10.7
11.6	0	0.71855	0.28145	−10.8	−10.3	−10.7
11.9	0	0.67757	0.32243	−10.7	−10.2	−10.6
			Wollast and Chou[66]			
1.2	0	0.99954	0.00046	−11.7		−13.5
2.2	0	0.99990	0.00010	−11.9	−13.0	−14.1
3.0	0	0.99977	0.00023	−12.3	−13.0	−13.8
4.0	0	0.99885	0.00115	−12.1	−12.9	−13.1
7.3	0	0.94755	0.05245	−11.3	−11.6	−11.4
8.9	0	0.87197	0.12803	−10.8	−10.9	−11.0
9.7	0	0.82851	0.17149	−10.6	−10.7	−10.9
11.1	0	0.74800	0.25200	−10.2	−10.4	−10.7
12.2	0	0.68279	0.31721	−10.0	−10.2	−10.6

[a] Obtained from ref 64.

inclusion of solvation effects lowers the barrier in protonated, neutral, and deprotonated reactions by 4, 12, and 20 kJ/mol, respectively. Comparing the gas-phase barrier heights in the present work to the previously reported data,[17,18] we find that the earlier data underestimate the barriers by about 28−33 kJ/mol in neutral and deprotonated calculations and overestimate by a same amount in the protonated case. The differences in the barriers could be attributed to the difference in the method and the basis set used for the calculations. However, as mentioned previously, the DFT method with larger MG3S is more appropriate than MP2 calculations with a smaller basis set.[55]

IV.B. Reaction Rate Constants. The rate constant calculations were performed on the basis of the gas-phase energetics data using only the smaller 6-31+G(d,p) basis set. The rate calculations using the MG3S basis set rate were not considered due to a higher relative expense of the rate constant calculations considering that the barrier height data were not significantly different from 6-31+G(d,p). The barrier heights estimated using the implicit solvation model do not allow the reoptimization of the gas-phase geometry and the frequencies, and therefore, rate constant calculations based on solvation data are not considered in the present work.

The rate constants were based on the implicit surfaces defined by electronic structure input files containing energies, gradients, and force constants (Hessians) of the reactants, products, and transition states geometries. Table 3 presents the rate constants (s^{-1}) for the protonated, neutral, and deprotonated reactions sites over the 200−500 K temperature range. As expected by the barrier heights of the two transition states in the protonated reaction site, the rate constant across the rate-limiting TS1 is several orders of magnitude smaller than that through TS2. A similar trend is evident in the deprotonated reaction where the rate constant for the TS1 is much smaller compared to the second transition state. The neutral reaction has only one transition state, and the value of the rate constant is lower than those of the protonated and deprotonated reactions.

IV.C. Reaction Rates as a Function of pH. The dissolution rates (mol m^{-2} s^{-1}) are calculated using the eq 3 for the 2−12 pH range at 298 K. The obtained rates are presented in Table 4 and compared to the dissolution of rates presented by Dove and Elston.[64] It is important to note that the rate model presented in ref 64 was fitted to the experimental data at 298 K. In addition, the measured experimental data by researchers were recalculated to 298 K if it was taken under different temperatures. Dove and Elston reported data from seven experimental studies; however, we limit our comparison to three of the seven experimental studies (perfomed by Knauss and Wolery, Schwartentruber et al., and Wollast and Chou). The remaining experiments were not chosen either because of a very narrow pH range or because of unclear experimental conditions. We use the site fraction data provided in ref 64 with the modification that in our work the deprotonated surface site fraction is considered as the sum of the deprotonated and sodium coordinated sites. This modification in our paper assumes that the electrostatic attraction between the sodium ions coordinated to the deprotonated sites does not alter the dissolution mechanism, and this assumption is in agreement with the discussion in ref 64. At this point, it is important to distinguish between the earlier theoretical work by Dove and Elston and the present work. In their work, the rate constant values were obtained by fitting the rate expression to the experimentally observed rates. However, in the present work *ab initio* calculations were performed and TST was used to compute the reaction rate constants.

The log(dissolution rate) vs the surface fraction of the deprotonated sites and pH is shown in Figure 4. It is evident

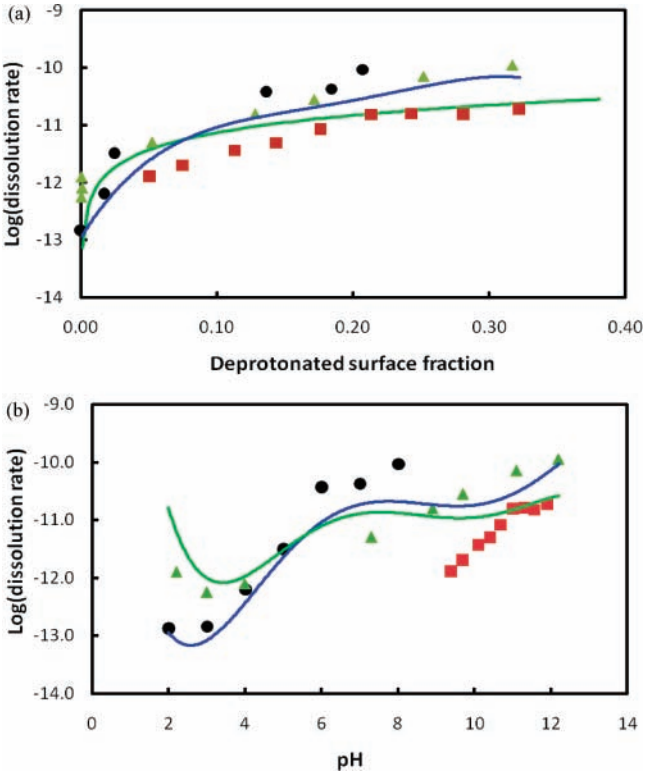

Figure 4. Log(dissolution rate) of quartz as a function of (a) deprotonated surface and (b) pH at 298 K. The dissolution rates calculated in the present work (green line) are compared to the empirically fitted rate model by Dove and Elston (blue line, ref 64) and the experimental studies reported therein by Knauss and Wolery (circles), Schwartentruber et al. (squares), and Wollast and Chou (triangles).

from the figure that all experiments do not span the entire pH range with Knauss and Wolery data limited to 2−8 pH range and Schwartentruber et al. data limited to 9−12 pH. A broader range of data over 2−12 pH was provided by Wollast and Chou; however, comparing their results to the other two experiments at the same pH yields different values of the rate. These variations in the experimental results can be attributed to the difference in experimental conditions. Dove and Elston first determined the fraction of various types of sites for each set of experimental conditions. They then fit the rates for each type of site to the experimental data to reproduce the overall trend in the dissolution rates over the entire pH range. We used the same correspondence between pH and the site fractions to obtain the dissolution rate as a function of pH (Figure 4b). In the examination of first the dissolution rate as a function of deprotonated surface fraction (Figure 4a), both the fitted Dove and Elston rates and our calculated rates track well the experimental data. For low pH values of ∼2 (Figure 4b), the rate is dominated by the slow neutral dissolution process. In the 2−4 pH range, the number of neutral sites decreases and the number of deprotonated sites remain sufficiently small as not to contribute to the dissolution. As the pH increases, the contribution from the faster dissolution deprotonated sites dominates the process. Both the Dove and Elston and our results show a local maximum in the dissolution rate at about pH = 7. This maximum is due to the assignment by Dove and Elston of the number of deprotonated sites for a given set of experimental conditions as evidence by the discontinuity in the rate at pH = 8 datum of Knauss and Wolery and the pH = 9.4 datum of Scwartentruber et al. The overall good agreement of our results with the previous experimental and fitted rates shows that the present approach is very successful in predicting the dissolution rates in quartz and can be extended to other minerals.

V. Conclusions

In this study, the quartz dissolution rates were calculated as a function of pH at 298 K. At a given pH the quartz surface reaction sites exist as a distribution of protonated, deprotonated, and neutral species. The dissolution mechanism for each of these three species was investigated by *ab initio* electronic structure calculations to obtain the reaction profile. The stationary points of the reaction profile were obtained by optimizing the geometric structures of the transition state(s), reaction intermediate (if any), and reactant and product complexes. The reaction profiles for the protonated and deprotonated species show similarity in the overall reaction profile with two transition states and a penta-coordinated intermediate. The transition state for the formation of this intermediate is the rate-limiting step with 69 and 110 kJ/mol barrier for protonated and deprotonated species. In contrast to these reaction profiles, the dissolution of the neutral species does not have a reaction intermediate but rather has a single transition state with 159 kJ/mol barrier height.

Using the barrier height and the partition functions for the transition state and the reactants in the rate-limiting steps, we calculated the TST rate constants for the reactions for the temperature range of 200−500 K. At 298 K the rate constant (s^{-1}) for the dissolution of neutral species was found to be 14 and 10 orders of magnitude smaller than the rate-limiting steps for the protonated and deprotonated species.

The values of the rate constants were used in the rate law expression together with the molar density of the surface reaction sites (mol m^{-2}) and the surface fractions of the protonated, neutral and deprotonated species at a given pH, to calculate the overall dissolution rate (mol m^{-2} s^{-1}). The obtained rates were compared to three previously reported experimental rates and one theoretically predicted rate obtained by fitting the data to the rate expression. Our values of the rates are in good agreement with the rates reported earlier. It is significant that the present *ab initio* approach provides good estimates of the dissolution rates without any kind of fitting technique. The method is capable of predicting the rates over the entire temperature range of 200−500 K for which the rate constant values are available. It is very encouraging that calculating the rate constant for a dissolution of a cluster of a mineral can be extended to the dissolution rates for the bulk of the mineral in experimental conditions.

The method presently does not take into account the connectivity of the surface reactive sites. In general, the reactive Si sites on the quartz surface differ in number of bridging oxygen atoms and the distribution of these sites varies from one crystallographic plane to the other. Using the distribution Si surface connectivity and the corresponding dissolution rate constant of silica cluster this method can be extended to predict the preferential dissolution of crystallographic planes in quartz.

Acknowledgment. We gratefully acknowledge the useful discussions with S. L. Brantley and K. T. Mueller on this work. This work has been supported by the National Science Foundation NSF under Grant Number CHE-0535656. We also thank The National Center for Supercomputing Applications (NCSA) for the computational resources under the TeraGrid Project Number TG-CHE070035N.

References and Notes

(1) Hering, J. G. *Oxidative and reductive dissolution*, 23rd ed.; Mineralogical Society of America: Wahington, DC, 1990.

(2) Iler, R. K. *The chemsitry of silica: solubility, polymerization, colloid and surface properties, and biochemitry*; Wiley Interscience: New York, 1979.
(3) Brinker, C. J.; Scherer, G. W. *Sol-Gel Science*; Academic Press: Boston, MA, 1990.
(4) Cundy, C. S.; Cox, P. A. *Chem. Rev.* **2003**, *103*, 663.
(5) Kawai, T.; Tsutsumi, K. *Colloid Polym. Sci.* **1998**, *276*, 992.
(6) Kirschhock, C. E. A.; Ravishankar, R.; Verspeurt, F.; Grobet, P. J.; Jacobs, P. A.; Martens, J. A. *J. Phys. Chem. B* **1999**, *103*, 4965.
(7) de Moor, P.-P. E. A.; Beelen, T. P. M.; van Santen, R. A.; Beck, L. W.; Davis, M. E. *J. Phys. Chem. B* **2000**, *104*, 7600.
(8) Bussian, P.; Sobott, F.; Brutschy, B.; Schrader, W.; Schuth, F. *Angew. Chem., Int. Ed.* **2000**, *39*, 3901.
(9) Knight, C. T. G.; Kinrade, S. D. *J. Phys. Chem. B* **2002**, *106*, 3329.
(10) Kirschhock, C. E. A.; Ravishankar, R.; Verspeurt, F.; Grobet, P. J.; Jacobs, P. A.; Martens, J. A. *J. Phys. Chem. B* **2002**, *106*, 3333.
(11) Felmy, A. R.; Cho, H.; Rustad, J. R.; Mason, M. J. *J. Solution Chem.* **2001**, *30*, 509.
(12) Pelster, S. A.; Schrader, W.; Schueth, F. *J. Am. Chem. Soc.* **2006**, *128*, 4310.
(13) Pokrovsky, O. S.; Golubev, S. V.; Mielczarski, J. A. *Colloid Interface Sci.* **2006**, *296*, 189.
(14) Yamabe, S.; Minato, T.; Hirao, K. *J. Chem. Phys.* **1984**, *80*, 1576.
(15) Kubicki, J. D.; Sykes, D. *Am. Mineral.* **1993**, *78*, 253.
(16) Kubicki, J. D.; Xiao, Y.; Lasaga, A. C. *Geochim. Cosmochim. Acta* **1993**, *57*, 3847.
(17) Xiao, Y.; Lasaga, A. C. *Geochim. Cosmochim. Acta* **1994**, *58*, 5379.
(18) Xiao, Y.; Lasaga, A. C. *Geochim. Cosmochim. Acta* **1996**, *60*, 2283.
(19) Pereira, J. C. G.; Catlow, C. R. A.; Price, G. D.; Almeida, R. M. *J. Sol-Gel Sci. Technol.* **1997**, *8*, 55.
(20) Pereira, J. C. G.; Catlow, C. R. A.; Pereira, J. C. G.; Price, G. D. *Chem. Commun.* **1998**, 1387.
(21) Pereira, J. C. G.; Catlow, C. R. A.; Price, G. D. *J. Phys. Chem. A* **1999**, *103*, 3268.
(22) Pereira, J. C. G.; Catlow, C. R. A.; Price, G. D. *J. Phys. Chem. A* **1999**, *103*, 3252.
(23) Pelmenschikov, A.; Strandh, H.; Pettersson, L. G. M.; Leszczynski, J. *J. Phys. Chem. B* **2000**, *104*, 5779.
(24) Pelmenschikov, A.; Leszczynski, J.; Pettersson, L. G. M. *J. Phys. Chem. A* **2001**, *105*, 9528.
(25) Yang, J.; Meng, S.; Xu, L. F.; Wang, E. G. *Phys. Rev. Lett.* **2004**, *92*, 146102.
(26) Tossell, J. A. *Geochim. Cosmochim. Acta* **2005**, *69*, 283.
(27) Mora-Fonz, M. J.; Catlow, C. R. A.; Lewis, D. W. *Angew. Chem., Int. Ed.* **2005**, *44*, 3082.
(28) Yang, J.; Wang, E. G. *Physical Rev. B* **2006**, *73*, 035406.
(29) Criscenti, L. J.; Kubicki, J. D.; Brantley, S. L. *J. Phys. Chem. A* **2006**, *110*, 198.
(30) Nangia, S.; Washton, N. M.; Mueller, K. T.; Kubicki, J. D.; Garrison, B. J. *J. Phys. Chem. C* **2007**, *111*, 5169.
(31) Gratz, A. J.; Bird, P. *Geochim. Cosmochim. Acta* **1993**, *57*, 977.
(32) Gratz, A. J.; Bird, P. *Geochim. Cosmochim. Acta* **1993**, *57*, 965.
(33) Siegel, D. I.; Pfannkuch, H. O. *Geochim. Cosmochim. Acta* **1984**, *48*, 197.
(34) Carroll-Webb, S. A.; Walther, J. V. *Geochim. Cosmochim. Acta* **1988**, *52*, 2609.
(35) Casey, W. H.; Westrich, H. R.; Holdren, G. R. *Am. Mineral.* **1991**, *76*, 211.
(36) Burch, T. E.; Nagy, K. L.; Lasaga, A. C. *Chem. Geol.* **1993**, *105*, 137.
(37) Mazer, J. J.; Walther, J. V. *J. Non-Cryst. Solids* **1994**, *170*, 32.
(38) Stillings, L. L.; Brantley, S. L. *Geochim. Cosmochim. Acta* **1995**, *59*, 1483.
(39) Stillings, L. L.; Drever, J. I.; Brantley, S. L.; Sun, Y.; Oxburgh, R. *Chem. Geol.* **1996**, *132*, 79.
(40) Chen, Y.; Brantley, S. L. *Chem. Geol.* **1997**, *135*, 275.
(41) Chen, Y.; Brantley, S. L. *Chem. Geol.* **2000**, *165*, 267.
(42) Oelkers, E. H.; Schott, J. *Geochim. Cosmochim. Acta* **2001**, *65*, 1219.
(43) Knauss, K. G.; Wolery, T. J. *Geochim. Cosmochim. Acta* **1987**, *52*, 43.
(44) Cypryk, M.; Apeloig, Y. *Organometallics* **2002**, *21*, 2165.
(45) Bunker, B. C.; Tallant, D. R.; Headley, T. J.; Turner, G. L.; Kirkpatrick, R. J. *Phys. Chem. Glasses* **1988**, *29*, 106.
(46) Truhlar, D. G.; Garrett, B. C. *Ann. Rev. Phys. Chem.* **1984**, *35*, 159.
(47) Hill, C. G. *An Introduction to Chemical Engineering Kinetics and Reactor Design*; Wiley: New York, 1977.
(48) Grinsven, j. J. M. v.; Riemsdijk, W. H. v. *Geoderma* **1992**, *52*, 41.
(49) Brantley, S. L. *Treatise Geochem.* **2004**, *5*, 73.
(50) Hayes, K. F.; Leckie, J. O. *J. Colloid Interface Sci.* **1987**, *115*, 564.
(51) Vosko, S. H.; Wilk, L.; Nusair, M. *Can. J. Phys.* **1980**, *58*, 1200.
(52) Lee, C.; Yang, W.; Parr, R. G. *Phys. Rev. B* **1988**, *37*, 785.
(53) Becke, A. D. *J. Chem. Phys.* **1993**, *98*, 5648.
(54) Stephens, P. J.; Devlin, F. J.; Chabalowski, C. F.; Frisch, M. J. *J. Phys. Chem. A* **1994**, *98*, 11623.
(55) Zhang, Y.; Li, Z. H.; Truhlar, D. G. *J. Chem. Theory Comput.* **2007**, *3*, 593.
(56) Frisch, M. J.; Pople, J. A. *J. Chem. Phys.* **1984**, *80*, 1384.
(57) Lynch, B. J.; Zhao, Y.; Truhlar, D. G. *J. Phys. Chem. A* **2003**, *107*, 1384.
(58) Curtiss, L. A.; Redfern, P. C.; Raghavachari, K.; Rassolov, V.; Pople, J. A. *J. Chem. Phys.* **1999**, *110*, 4703.
(59) Fast, P. L.; Sanchez, M. L.; Truhlar, D. G. *Chem. Phys. Lett.* **1999**, *306*, 407.
(60) Frisch, M. J.; Trucks, G. W.; Schlegel, H. B.; Scuseria, G. E.; Robb, M. A.; Cheeseman, J. R.; Montgomery, J. A., Jr.; Vreven, T.; Kudin, K. N.; Burant, J. C.; Millam, J. M.; Iyengar, S. S.; Tomasi, J.; Barone, V.; Mennucci, B.; Cossi, M.; Scalmani, G.; Rega, N.; Petersson, G. A.; Nakatsuji, H.; Hada, M.; Ehara, M.; Toyota, K.; Fukuda, R.; Hasegawa, J.; Ishida, M.; Nakajima, T.; Honda, Y.; Kitao, O.; Nakai, H.; Klene, M.; Li, X.; Knox, J. E.; Hratchian, H. P.; Cross, J. B.; Bakken, V.; Adamo, C.; Jaramillo, J.; Gomperts, R.; Stratmann, R. E.; Yazyev, O.; Austin, A. J.; Cammi, R.; Pomelli, C.; Ochterski, J. W.; Ayala, P. Y.; Morokuma, K.; Voth, G. A.; Salvador, P.; Dannenberg, J. J.; Zakrzewski, V. G.; Dapprich, S.; Daniels, A. D.; Strain, M. C.; Farkas, O.; Malick, D. K.; Rabuck, A. D.; Raghavachari, K.; Foresman, J. B.; Ortiz, J. V.; Cui, Q.; Baboul, A. G.; Clifford, S.; Cioslowski, J.; Stefanov, B. B.; Liu, G.; Liashenko, A.; Piskorz, P.; Komaromi, I.; Martin, R. L.; Fox, D. J.; Keith, T.; Al-Laham, M. A.; Peng, C. Y.; Nanayakkara, A.; Challacombe, M.; Gill, P. M. W.; Johnson, B.; Chen, W.; Wong, M. W.; Gonzalez, C.; Pople, J. A. *Gaussian 03*, revision C.02; Gaussian, Inc.: Wallingford, CT, 2004.
(61) Cancès, E.; Mennucci, B.; Tomasi, J. *J. Chem. Phys.* **1997**, *107*, 3032.
(62) Corchado, J. C.; Chuang, Y.-Y.; Coitiño, E. L.; Truhlar, D. G. GAUSSRATE, 9.4 ed.; University of Minnesota: Minneapolis, MN, 2003.
(63) Corchado, J. C.; Chuang, Y.-Y.; Fast, P. L.; Hu, W.-P.; Liu, Y.-P.; Lynch, G. C.; Nguyen, K. A.; Jackels, C. F.; Ramos, A. F.; Ellingson, B. A.; Lynch, B. J.; Melissas, V. S.; Villà, J.; Rossi, I.; Coitiño, E. L.; Pu, J.; Albu, T. V.; Steckler, R.; B. C. Garrett; Isaacson, A. D.; Truhlar, D. G. POLYRATE−version 9.4; University of Minnesota: Minneapolis, MN, 2005.
(64) Dove, P. M.; Elston, S. F. *Geochim. Cosmochim. Acta* **1992**, *56*, 4147.
(65) Schwartzentruber, J.; Furst, W.; Renon, H. *Geochim. Cosmochim. Acta* **1987**, *51*, 1867.
(66) Wollast, R.; Chou, L. In *NATO ASI Series, No. 251*; Lerman A., Meybeck, M., Eds.; NATO: Geneva, 1988.